GLOBAL VECTOR FIELD RECONSTRUCTION OF CHAOTIC ATTRACTORS FROM ONE UNSTABLE PERIODIC ORBIT

C. Letellier, E. Ringuet, J. Maquet, B. Maheu, G. Gouesbet
Laboratoire d'Energétique des Systèmes et Procédés
URA CNRS 230, INSA de Rouen,
BP 08, 76 130 Mont-Saint-Aignan,
France

All the information necessary to build a chaotic attractor may be retrieved from the knowledge of a single unstable periodic orbit. This statement is illustrated by achieving a global vector field reconstruction of the Rössler system from a period-1 orbit. Similarly, it is shown that an intermittent behaviour may be reconstructed by knowing only the laminar phases.

Reconstruction globale de champs de vecteurs d'attracteurs chaotiques à partir d'une orbite périodique instable

L'ensemble de l'information nécessaire à la construction d'un attracteur chaotique peut être extraite de la connaissance d'une simple orbite périodique instable. Cette proposition est illustrée par une reconstruction globale d'un champ de vecteurs du système de Rössler à partir d'une orbite de période 1. Selon cette technique, il est montré qu'un régime intermittent peut être reconstruit à partir des phases laminaires.

1. INTRODUCTION

An approach of great interest for the characterization of dynamical systems is devoted to the portrait reconstruction from a scalar time series initiated by Packard et al [1]. A more general approach is devoted to global vector field reconstructions defined as follows. Given a scalar time series for an observable, provide a set of ordinary differential equations equivalent to the original underlying system. There is a great deal of interest in this problem ([2] and references therein). In this framework, the natural question is to ask how many unstable periodic orbits are necessary to achieve a global vector field reconstruction. This paper shows that the answer is 1.

The paper is organized as follows. Section 2 gives a brief presentation of the global vector field reconstruction of the Rössler system from the y-time series. Section 3 gives an example of successful reconstruction from one periodic orbit for different values of a control parameter. A qualitative discussion concerning the information contained in the orbit allows to understand this fact for the Rössler system. Section 4 is devoted to the case of an intermittent behaviour where the laminar regime is very close to a period-3 orbit. It is then shown that the intermittent dynamics may be retrieved by knowing only the laminar behaviour. Section 5 gives a conclusion.

2. GLOBAL VECTOR FIELD RECONSTRUCTION

State space reconstruction is the creation of multidimensional, deterministic state space from a time series. Let us start from a 3D time continuous dynamical system given by the Rössler system which reads as :

$$\begin{cases} \dot{x} = -y - z \\ \dot{y} = x + ay \\ \dot{z} = b + z(x - c) \end{cases} \quad (1)$$

with a control parameter vector (a, b, c). It is assumed that the observer numerically (or experimentally) recorded a scalar time signal, here taken to be $y(t)$. A reconstructed state space may be equivalently spanned by delay coordinates or derivative coordinates [3]. Only derivative coordinates are here considered. The aim is then to reconstruct a vector field equivalent to the original system under the form of a standard system [2] made of the observable and its derivatives. From the y-variable of the Rössler system, we found :

$$\begin{cases} \dot{Y} = Z \\ \dot{Z} = X \\ \dot{X} = F_y(X, Y, Z) \end{cases} \quad (2)$$

in which standard coordinates (X, Y, Z) are the derivatives $(\ddot{y}, y, \dot{y})$. F_y is a function of the derivative coordinates here called the standard function which may be

mots-clés • keywords thermodynamique des systèmes complexes • mécanique des fluides • attracteurs chaotiques • orbite périodique instable • reconstruction globale de champs de vecteur
complex thermodynamical system • fluid mechanics • chaotic attractors • unstable periodic orbit • global vector field reconstruction

reconstructed by using a multivariate polynomial approximation on nets [2]. This approximation technique is presented in the appendix A. The approximated standard function $\tilde{F}_y$ may be written as :

$$\tilde{F}_y = \sum_{p=1}^{n} K_p P^p \qquad (3)$$

where P^p designates the multivariate terms $X^i Y^j Z^k$ (see the appendix).

In order to evaluate the coefficients K_p, reconstruction parameters must be introduced [2]. They are a time interval δt used to evaluate derivatives, the number of points N_q taken on the net, the number of points N_s sampled per pseudo-period T_0, and n the number of polynomials in the standard function approximation. The vector $(\delta t, N_q, N_s, n)$ is called the reconstruction or driving vector.

When the original system is known, a *standard transformation* Φ expressing the standard coordinates (X, Y, Z) versus the original coordinates (x, y, z) may be obtained according to [2] :

$$\Phi \equiv \begin{cases} X = ax + (a^2 - 1)y - z \\ Y = y \\ Z = x + ay \end{cases} \qquad (4)$$

in the case where the y-variable of the Rössler system constitutes the recorded time series.

The *standard function* F_y is then found to be [2] :

$$F_y = -b - cY + (ac - 1)Z + (a - c)X$$
$$-aY^2 + (a^2 + 1)YZ - aXY - aZ^2 + XZ \qquad (5)$$

This is a very simple case where the standard function F_y is a polynomial function and may be exactly expanded on E^9 (see the appendix). In such a case, the natural spectrum of $K_p's$ may be obtained versus the control parameters (Table 1). The solutions of the reconstruction method are then very robust against changes of reconstruction parameters [2], allowing us to investigate opportunities without being worried by accessory technicalities. In particular, successful reconstructions may be obtained with a driving vector (10^{-3}, 10, 10, 10,) as shown in Ref [2]. Furthermore, it can easily be shown that the standard transformation Φ defines a diffeomorphism between the original system and the standard system, i.e. all the information about the dynamics is preserved, including in particular topological equivalence.

p		K_p		$\tilde{K}_p$
1	$-b$	=	-2	-1.999921
2	$-c$	=	-4	-3.999950
3	$ac-1$	=	0.7318	0.731773
4	$a-c$	=	-3.56705	-3.566983
5	$-a$	=	-0.43295	-0.432967
6	a^2+1	=	1.187445703	1.187429
7	$-a$	=	-0.43295	-0.43295
8	$-a$	=	-0.43295	-0.432944
9		1		0.999980

Table 1. K_p's expressions versus control parameters of the Rössler system. Note that the K_p-spectrum is defined with standard coordinates (Y, Z, X) taken in that order, according to Rel. (4). Hence, for instance K_2 is $(-c)$, not the coeffficient $(a - c)$ of the monomial X. Estimated values $\tilde{K}_p$'s for $a = 0.43295$ are also given

We will now focus our purpose on reconstruction of equivalent vector fields from y-time series of the Rössler system.

3. RECONSTRUCTION FROM ONE PERIODIC ORBIT

As in Ref [4], the Rössler system is studied on the control parameter line (a, b, c) = (variable, 2, 4). Three different dynamical behaviours may then be distinguished (i) the spiral-type ($a = 0.43295$) (ii) the funnel-type ($a = 0.523$) which must be described by using a 4-letter symbolic dynamics and (iii) a type-I intermittency for $a \approx 0.409$. Cases (i) and (ii) are discussed in this section while the intermittent behaviour is considered in section 4.

A. Topology

For $a = 0.43295$, the asymptotic behaviour settles down on a strange chaotic attractor which is characterized by a two strand template given in Fig. 1.a, achieving the topological characterization of the attractor [4]. A similar study will be carried out for a more developed chaos ($a = 0.523$) for which the asymptotic behaviour settles down on a strange chaotic attractor which is characterized by a four strand template (Fig. 1.b), in relation with the fact that the first-return map presents four monotonic branches [4].

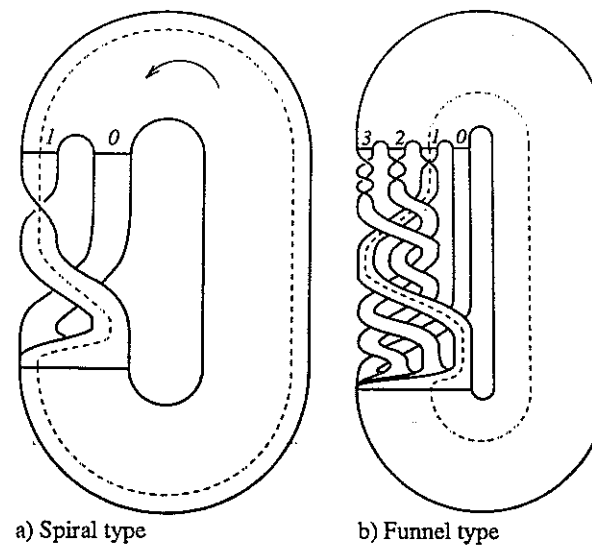

a) Spiral type b) Funnel type

Fig. 1 Template of the Rössler system : the spiral type ($a = 0.43295$) and the funnel type ($a = 0.523$) Period-1 orbit encoded by (1) is constructed on each template.

B. Reconstruction

We now proceed to a global vector field reconstruction by considering that the observable is the variable y (section 2). Furthermore, the time series is chosen to be taken from the periodic orbit encoded by (1), topologically represented in Fig. 1. This period-1 orbit may be obtained by integrating the Rössler system (1) starting from the initial conditions [4] :

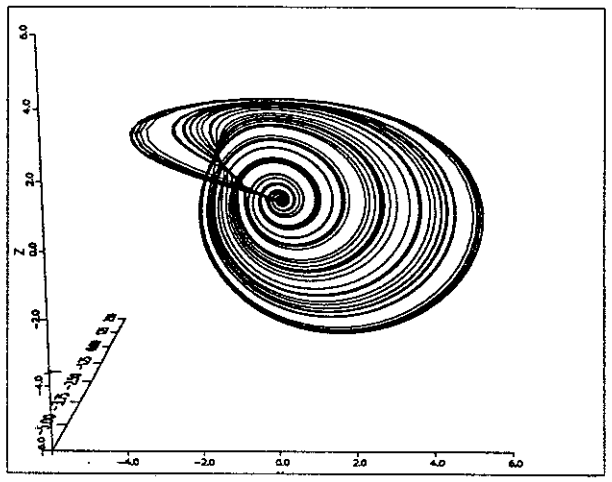

Fig. 2 Reconstructed attractor from the periodic orbit encoded by (1) with the driving vector (10^{-3}, 20, 10, 10) for $a = 0.43295$

$$\begin{cases} x_0 = 0.2296610494032504 \\ y_0 = -4.11575770590046 \\ z_0 = 0.4500602426204998 \end{cases} \quad (6)$$

which define a point of the periodic orbit (1) for $a = 0.43295$. With the number of digits given in Rel (6) to represent the initial conditions, the trajectory remains on the unstable periodic orbit for about ten pseudo-periods T_0 before being ejected out of it. The driving vector is taken to be (10^{-3}, 20, 10, 10) , achieving a sampling over two pseudo-periods, ensuring us that the reconstruction is generated only by points on the orbit. A successful reconstruction is then obtained. Reconstructed K_p -values are reported in Table 1, in excellent agreement with theoretical values. The chaotic attractor generated by the reconstructed system is represented on Fig. 2.

The first-return map (Fig. 3) is similar to the original map [4] since the increasing branch indeed adjoins the bissectrix line. We found that the reconstructed attractor is topologically equivalent to the original attractor, i.e. the chaotic attractor has successfully been reconstructed from a single period-1 orbit.

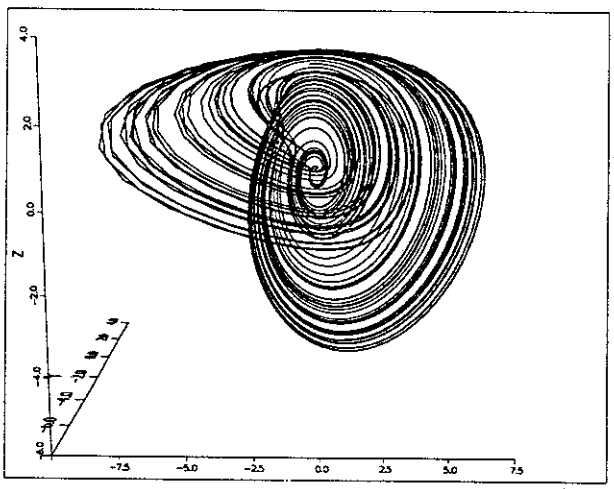

Fig. 4 Reconstructed attractor from the periodic orbit encoded by (1) with the driving vector (10^{-3}, 20, 10, 10) for $a = 0.523$

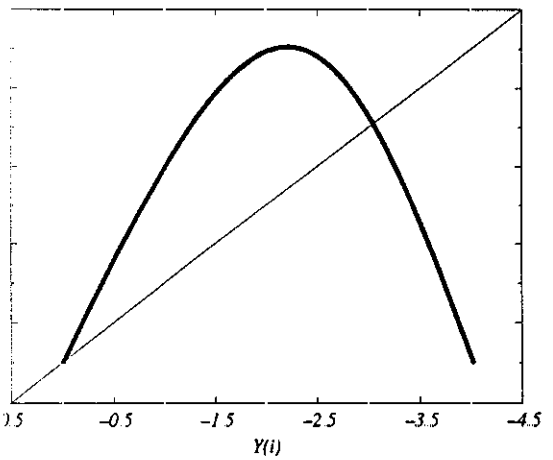

Fig. 3 First-return-map associated with the reconstructed attractor

C. Funnel type

A successful reconstruction is also obtained from the orbit (1) with the same driving vector as in the previous subsection. K_p-estimated values are reported in Table 2 showing again a very good agreement between original and reconstructed values. Furthermore, the reconstructed standard system again generates an attractor which is topologically equivalent to the original one (Fig. 4), and the associated Poincaré map is constituted by four monotonic branches (Fig. 5) as on the original attractor [4].

p	K_p	$\tilde{K}_p$
1	- 2	- 2.000021
2	- 4	- 3.999869
3	1.092	1.091931
4	- 3.477	- 3.476880
5	- 0.523	- 0.523052
6	1.273529	1.273502
7	- 0.523	- 0.523082
8	- 0.523	- 0.522953
9	1	0.999953

Table 2. Theoretical values and estimated values of $\tilde{K}_p$'s for $a = 0.523$

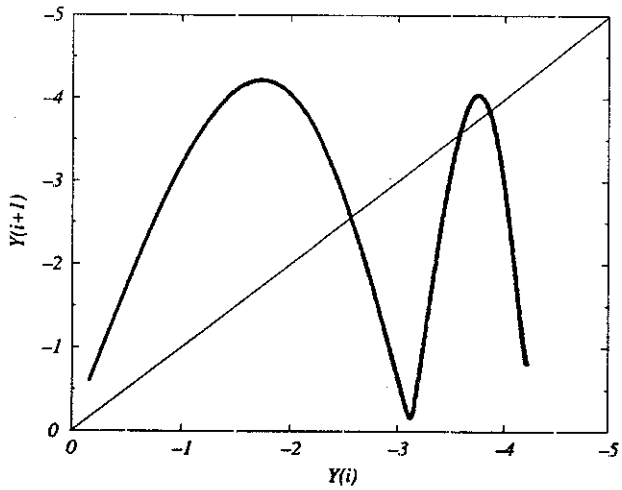

Fig. 5 First-return map associated with the reconstructed attractor. Four monotonic branches are present as on the original Poincaré map

D. Discussion

It has been demonstrated in section (3) that successful global vector field reconstructions may be carried out by relying only on the knowledge of the period-1 orbit encoded by the sequence (1).

Actually, such a success is not very surprising in so far as we have used a differential embedding. It essentially results from the smoothness of the vector field. Another point of view is to consider Rel (5) exhibiting 9 different values of K_p's. Therefore, evaluating $\dot{Z}_i$ for nine different locations is in principle sufficient to recover the K_p-spectrum. In principle again, any small portion of the period-1 orbit (1), or of any piece of a chaotic trajectory, or even of a small piece of a transient behaviour, is enough to carry out a successful global differential vector field reconstruction. Such features are certainly a privilege of differential embeddings when compared to time-delay embeddings.

In practice however, the success of a global vector field reconstruction from a small portion of a trajectory should, for numerical reasons, depend very much on the pertinence of the differential information contained in this portion, i.e. robustness of the reconstruction should depend on the amount and on the nature of the information contained in this portion, in relation with its modification through a change of the control parameter. This issue is now qualitatively discussed.

Orbits (1) for $a = 0.43295$ and $a = 0.523$ do not contain the same information since they allow the reconstruction of different attractors by using a global vector field reconstruction. In order to exhibit the evolution of orbit (1), let us study its geometrical properties. The Rössler system (1) possesses two fixed points F_+ and F_- given by :

$$\left(x_\pm = \frac{c_\pm \left(c^2 - 4ab\right)^{1/2}}{2}, y_\pm = \frac{-x_\pm}{a}, z_\pm = \frac{x_\pm}{a} \right)$$

A 2D unstable manifold is associated with F_- : trajectories in this manifold spiral outward from F_- [5]. The stable manifold is unidimensional. With the second fixed point F_+ are associated a unidimensional unstable manifold and a 2D stable manifold on which trajectories spiral inward to F_+. This stable manifold faces the folding region of the attractor in such a way that folding may be associated with the rotation produced by F_+.

Consequently, one vortex may be associated with each fixed point. Each vortex is characterized by an angular speed w_+ and w_- for F_+ and F_-, respectively. These quantities are determined by solving the characteristic polynomial of the Jacobian given by :

$$-\lambda^3 + (a + x - c)\lambda^2 + x - c + az + (ac - ax - 1 - z)\lambda = 0 \qquad (7)$$

at F_- and F_+. The eigenvalues are found to read as :

$$\begin{cases} \rho_- \pm i w_- = 0.1481087 \pm i 0.975955 \\ -\lambda_- = -3.63360630 \end{cases}$$

and

$$\begin{cases} \rho_+ \pm i w_+ = -0.08145529 \pm i 3.108388 \\ \lambda_+ = 0.36619954 \end{cases}$$

Let us remark that the value of the pseudo-period T_0 may be approximatively evaluated as :

$$T_0 \approx \frac{2\pi}{w_-} = 6.43\ s \qquad (8)$$

By inspecting the values ρ_- and w_-, the original Hopf bifurcation is found to arise for $a_H = 0.12496$ for which we have then $\rho_- \approx 0$ and $w_- \approx 1$. For this a-value, the first limit cycle is born, namely orbit (1). A bit beyond a_H, orbit (1) is essentially driven by the vortex associated with F_- and describes an ellipsis which is contained in a surface approximatively plane and parallel to the plane (xy).

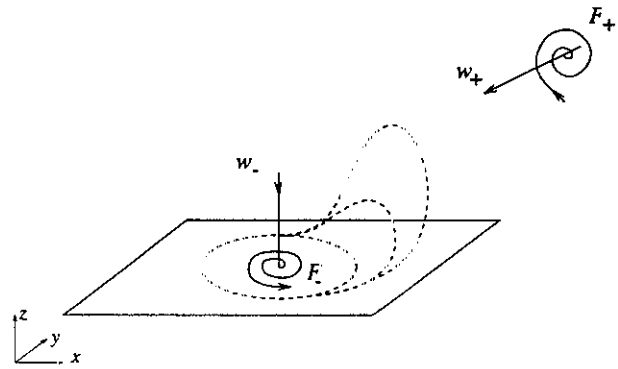

Fig. 6 Evolution of orbit (1) : a part of it leaves progressively the original plane following the z-direction under the increasing influence of the vortex associated with F_+

As the parameter a is increased, the fixed point F_+ comes closer to F_-. Its vortex becomes more influent on the attractor and, consequently, on orbit (1), i.e. a part of orbit (1) leaves progressively the original plane in the z-direction (Fig. 6). Then, its differential structure changes and both its length and time period T (1) grow. It then appears that T (1) is a monotonic signature of the differential structure of orbit (1) as displayed in Fig. 7, showing T (1) versus a. Therefore, a sufficient information related to orbit (1) is exhibited. The information necessary to global vector field reconstruction is of a differential nature.

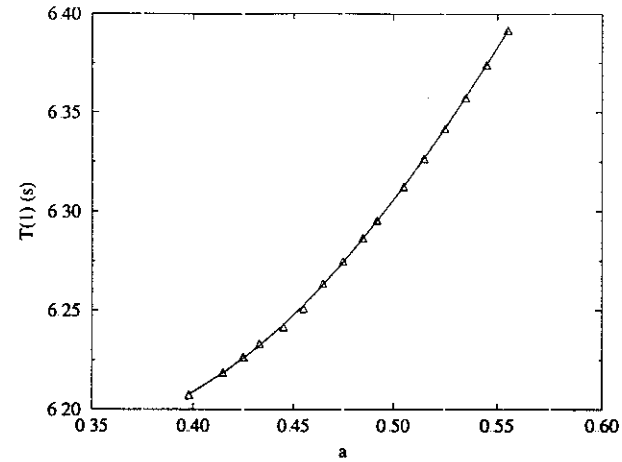

Fig. 7 Evolution of the time period T (1) versus the a values

4. INTERMITTENT BEHAVIOUR

An intermittent behaviour may be decomposed into laminar phases, where the dynamics remains see-

mingly periodic during long time intervals, and bursts abruptly disrupting the regular behaviour. The laminar phases are very close to a periodic orbit. Therefore, it is expected that we should be able to reconstruct an equivalent vector field from laminar phases only, in a way similar as from period-1 orbits in the previous section.

A. Type-I intermittency

This behaviour appears before a tangent bifurcation which will imply the birth of a limit cycle and of an unstable periodic orbit [6]. It takes the form of laminar phases where the trajectory is very close to the limit cycle, interrupted by chaotic bursts. The averaged length $\bar{L}$ of the laminar phases evolves according to :

$$\bar{L} \propto \varepsilon^{-\alpha} \qquad (9)$$

where ε represents a distance to the tangent bifurcation and α is equal to 1/2 [7].

Hirsch et al [7] have shown that the type-I intermittency appears in the logistic map just before the creation of a limit cycle of period 3. They characterize this behaviour by the probability distribution $P(L)$ of the length L of laminar phases.

Similarly as for the logistic map, the Rössler system presents a tangent bifurcation before the apparition of the limit cycle of period 3 [8] for $a = a_c = 0.4091200$ ($b = 2$, $c = 4$). If a is greater than a_c, the asymptotic behaviour is a limit cycle of period 3 and, consequently, the time series of the observable y exhibits three different minima, here called y_1, y_2 and y_3 in a decreasing order. Consequently, y_3 is the smallest minimum. For $a < a_c$, in a laminar phase, the smallest minimum $y_{min}(t)$ of the y -time series evolves in the neighborhood of y_3. In order to define the laminar regions, we introduce an acceptance criterion on deviations of $y_{min}(t)$ according to :

$$y_{min}(t) - y_3 \leq k(y_1 - y_3) \qquad (10)$$

where k must be small. It is arbitrarily chosen equal to 2/100. If this condition is realized, asymptotic behaviour is very close to the limit cycle and, consequently, is on a laminar phase ; if it is not, then the evolution corresponds to a burst. The evolution of the maximum laminar phase length L_{max} versus ε is represented by the dashed line in Fig. 8. This evolution is in agreement with Rel. (9) in which α is found to be equal to 0.53 ± 0.01, very close to the theoretical value [7]. The probability distribution $P(L)$ is represented in Fig. 9.a evidencing the existence of two principal characteristic lengths for short and long laminar phases in agreement with the behaviour exhibited by Hirsch et al in the case of the logistic map.

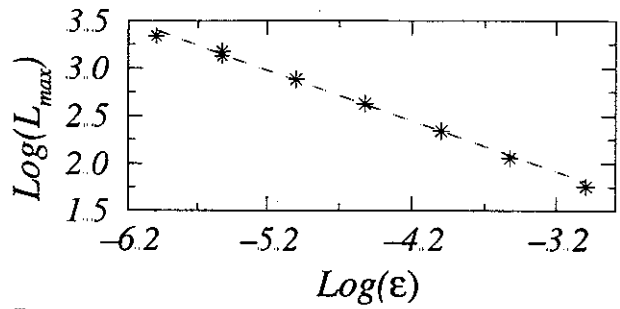

*Fig. 8 Evolution of the maximum laminar phase length L_{max} Dashed line : original system, * : reconstructed system*

B. Reconstructed intermittency

A reconstruction of a global vector field equivalent to the Rössler system is now carried out with the same method than in section 3. We have stated in section 2 that a satisfactory reconstruction is feasible with only $N_q = 10$ points on the net. For the intermittency case however, the results depend on the location of the net points along the trajectory. It then appears that, with a driving vector (10^{-3}, 10,10, 10), three kinds of reconstructed asymptotic behaviour may be observed depending on the runs~: i) chaotic behaviour without any laminar phase, ii) intermittent behaviour with laminar phases during from 200 s up to 1000 s, in contrast with the fact that the maximum length of laminar phases is about 190 s for the original system and iii) a limit cycle of period 3 or 9.

The values of the K_p-coefficients K_5, K_7 and K_8 are the most sensitive with respect to the location of the net points. However, all these side effects are killed with a driving vector (10^{-3}, 20, 10, 10) , i.e. with N_q =20 instead of $N_q = 10$. The maximum length L_{max} of the reconstructed regime is computed versus ε and displayed in Fig. 8, in very good agreement with the results from the original system. Such reconstructions work indifferently as well for points taken from the laminar phases or from chaotic bursts. When ε becomes very small ($\varepsilon \leq 10^{-6}$), N_q must however be increased up to 30 to

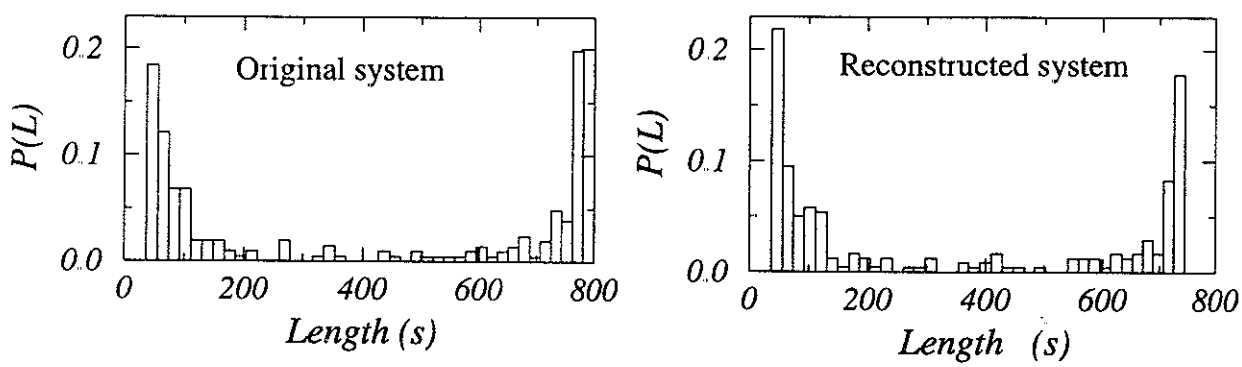

Fig. 9 Probability distribution P (L)

a) the original system : (a, b, c) = (0.40911, 2, 4), i.e. $\varepsilon = 10^{-5}$. This is a Type-I intermittency (200 laminar phases are taken into account)

b) the reconstructed system with the driving vector (10^{-3},20,10,10) : (a, b, c) = (0.40911, 2, 4). P (L) is very close to the one associated with the original system

avoid limit cycle reconstruction instead of intermittent behaviour reconstruction. For $\varepsilon = 10^{-5}$ (a = 0.40911), the probability distribution $P(L)$ of laminar phase length L is computed for the reconstructed system with the driving vector (10^{-3},2 0, 10, 10) with points choosen in a laminar phase and displayed in Fig. 9.b. The agreement between the original system (Fig. 9.a) and the reconstructed system (Fig. 9.b) is very good, except that the maximum length is slightly underestimated in the reconstructed system.

5. CONCLUSION

It has been demonstrated that a very small amount of information is sufficient to reconstruct a vector field equivalent to the vector field of the original underlying system. In the Rössler case, a period-1 orbit encoded by (1) provides a sufficient knowledge about the dynamics to recover the complete attractor by using a global vector field reconstruction method with derivative coordinates. We explain such powerful results in terms of the differential structure which is taken into account by derivatives. Another example concerns the study of a type-I intermittency. The reconstruction is successfully achieved from a small amount of data taken from the laminar phases. We believe that such results should encourage us to a systematic study of differential embeddings and reconstructions which have been underdeveloped when compared to delay techniques. Let us note that these techniques may be applied to experimental systems, as for the study of electrodissolution [9] [10] or the characterization of Cepheïde stars. In the last case, it has been shown that the complex thermodynamical system constituted by such a star reduces to a dynamical system with three degrees of freedom [11].

Bibliography

[1] Packard N. H., Crutchfield J. P., Farmer J. D., Shaw R. S., *"Geometry from a time series"*, Phys. Rev. Lett., 45 (9), 712-716, (1980).

[2] Gouesbet G., Letellier C., *"Global vector field reconstruction by using a multivariate polynomial L2-approximation on nets"*, Phys. Rev. E, 49 (6), 4955-4972, (1994).

[3] Gibson J F., Farmer J. D., Casdagli M., Eubank S., *"An Analytic Approach to Practical State Space Reconstruction"*, Physica D, 57, 1-30, (1992).

[4] Letellier C., Dutertre P., Maheu B., *"Unstable periodic orbits and templates of the Rössler system : toward a systematic topological characterization"*, Chaos, 5 (1), 271-282, (1995).

[5] Thompson J. M. T., Stewart J. M., *"Nonlinear Dynamics and Chaos"*, John Wiley & Sons, (1986).

[6] Manneville P., Pomeau Y., *"Intermittency and the Lorenz model"*, Phys. Lett., 57A (1), 2, (1979).

[7] Hirsch J. E., Huberman B. A., Scalapino D. J., *"Theory of intermittency"*, Phys. Rev. A, 25 (1), 519-532, (1982).

[8] Fraser S., Kapral R., *"Analysis of flow hysteresis by a one-dimensional map"*, Phys. Rev. A, 25 (6), 3223-3233, (1982).

[9] Letellier C., Le Sceller L., Maréchal E., Dutertre P., Maheu B., Gouesbet G., Fei Z., Hudson J. L., *"Global vector field reconstruction from a chaotic experimental signal in copper electrodissolution"*, Physical Review E, 51 (5), 4262-4266, (1995)

[10] Letellier C., Le Sceller L., Dutertre P., Gouesbet G., Fei Z., Hudson J. L., *"Topological Characterization and Global Vector Field Reconstruction from experimental electrochemical system"*, Journal of Physical Chemistry, 99, 7016-7027, (1995).

[11] Letellier C., Gouesbet G., Soufi F., Buchler J. R., Kolláth Z., *"Chaos in variable stars : topological analysis of W Vir model pulsations"*, Chaos, 6, 3, 466-476, (1996).

Appendix A

Approximation on a multivariate polynomial basis

1. Functional space E^n

The function F is projected on a space E^n of polynomials. These polynomials depend on the derivative coordinates (X_1, X_2, X_3), therefore involving terms reading (X_1^i, X_2^j, X_3^k). As detailed in Ref. [2], we first define monomials P^n by considering the ordering of triplets (i, j, k) :

$$\begin{cases} 000 \\ 100\ 010\ 001 \\ 200\ 110\ 101\ 020\ 011\ 002 \\ \dots \end{cases} \tag{A1}$$

which are numbered by taking the natural numbers $n \in N$ in the same ordering :

$$\begin{cases} 1 \\ 2\ \ 3\ \ 4 \\ 5\ \ 6\ \ 7\ \ 8\ \ 9\ \ 10 \\ \dots \end{cases} \tag{A2}$$

defining a one-to-one relationship between triplets (i, j, k) and natural numbers $n \in N$. Then the following convenient notation is introduced to define the monomials P^n :

$$P^n = X^i Y^j Z^k \tag{A3}$$

Vectorial space E^n is constituted by the linear relations on monomials P^i such that $i \leq n$, i.e. a basis of E^n is $\{P^i\}$. We afterward build an orthonormal basis $\{\phi^k\}$ from the basis $\{P^i\}$.

2. Orthonormal basis

In this paper, the basis $\{\phi^k\}$ is built by using a Gram-Schmidt orthogonalization procedure, leading to a somewhat more compact formulation than in Ref. [2]. According to this procedure, the functions ϕ^k read as :

$$\phi^k = \frac{\phi^{*k}}{\left\| \phi^{*k} \right\|} \tag{A4}$$

in which elements ϕ^{*k} are defined as :

$$\begin{cases} \phi^{*1} = P^1 \\ \phi^{*k} = P^k - \sum_{\alpha=1}^{k-1} \left(P^k, \phi^\alpha \right) \phi^\alpha, k > 1 \end{cases} \tag{A5}$$

in which $(\ ,\ )$ designates a scalar product. The orthonormality condition reads as :

$$\left(\phi^i, \phi^j \right) = \delta_{ij} \tag{A6}$$

where δ_{ij} is the Kronecker symbol. Rels (A4) and (A5) imply that ϕ^k's define a multivariate triangular family of polynomials given by :

$$\begin{cases} \phi^1 = A_1^1 \\ \phi^2 = A_1^2 + A_2^2 X \\ \phi^3 = A_1^3 + A_2^3 X + A_3^3 Y \\ \phi^4 = A_1^4 + A_2^4 X + A_3^4 Y + A_4^4 Z \\ \phi^5 = A_1^5 + A_2^5 X + A_3^5 Y + A_4^5 Z + A_5^5 X^2 \\ \dots \end{cases}$$

The projection of a monomial P^k on the orthonormal basis $\{\phi^j\}$ reads as :

$$P^k = \sum_{\alpha=1}^{k} B_\alpha^k \phi^\alpha \qquad \text{(A7)}$$

The expansion coefficients B_α^k then read as :

$$B_\alpha^k = \left(P^k, \phi^\alpha\right) \qquad \text{(A8)}$$

Conversely, each function ϕ^k may be expanded on the basis $\{P^j\}$ according to :

$$\phi^k = \sum_{\alpha=1}^{k} A_\alpha^k P^\alpha \qquad \text{(A9)}$$

Therefore, coefficients B_j^k also read as :

$$B_j^k = \sum_{\alpha=1}^{j} A_\alpha^j \left(P^k, P^\alpha\right) \qquad \text{(A10)}$$

Inserting Rels (A8) and (A9) in Rel. (A5), we obtain :

$$\begin{cases} \sum_{\alpha=1}^{k} A_\alpha^{*k} P^\alpha = P^k - \sum_{\beta=1}^{k-1} B_\beta^k \sum_{\alpha=1}^{\beta} A_\alpha^\beta P^\alpha \\ A_\alpha^{*k} = A_\alpha^k \left\| \phi^{*k} \right\| \end{cases} \qquad \text{(A11)}$$

With a permutation on the sums :

$$\sum_{\beta=1}^{k-1} \sum_{\alpha=1}^{\beta} = \sum_{\alpha=1}^{k-1} \sum_{\beta=\alpha}^{k-1} \qquad \text{(A12)}$$

we obtain :

$$\sum_{\alpha=1}^{k} A_\alpha^{*k} P^\alpha = P^k - \sum_{\alpha=1}^{k-1} \left(\sum_{\beta=\alpha}^{k-1} B_\beta^k A_\alpha^\beta \right) P^\alpha \qquad \text{(A13)}$$

leading to the following recurrence relations :

$$\begin{cases} A_k^{*k} = 1 \\ A_\alpha^{*k} = -\sum_{\beta=\alpha}^{k-1} B_\beta^k A_\alpha^\beta \qquad \text{for } \alpha < k \end{cases} \qquad \text{(A14)}$$

Coefficients B_β^k may then be substituted in terms of coefficients A_i^j by using Rel (A10), leading to :

$$A_\alpha^{*k} = -\sum_{\beta=\alpha}^{k-1} A_\alpha^\beta \left[\sum_{\gamma=1}^{\beta} A_\gamma^\beta \left(P^k, P^\gamma\right) \right] \qquad \text{(A15)}$$

Finally, once the coefficients A_α^{*k} are obtained, we may evaluate the coefficients A_α^k of the orthonormal basis by using :

$$A_\alpha^k = \frac{A_\alpha^{*k}}{\left[\sum_{\beta=1}^{k} \sum_{\gamma=1}^{k} A_\beta^{*k} A_\gamma^{*k} \left(P^\beta, P^\gamma\right) \right]^{1/2}} \qquad \text{(A16)}$$

3. Fourier approximation

At this step, we possess a complete basis of n orthonormal polynomials ϕ^k. We then look for an approximation $\tilde{F}$ of the standard function F, knowing the values of F on a net (X_i, Y_i, Z_i), in which the net is formed from the values of standard coordinates at discrete times i, i.e. for instance :

$$F\left(X_i, Y_i, Z_i\right) = \dot{Z}_i \qquad \text{(A17)}$$

The best L_2 -approximation (in the least square sense) is given by :

$$\tilde{F} = \sum_j c_j^* \phi^j \qquad \text{(A18)}$$

in which c_j^* are the Fourier coefficients reading as :

$$c_j^* = \left(F, \phi^j\right) \qquad \text{(A19)}$$

We thus have :

$$c_j^* = \left(\dot{Z}_i, \sum_{k=1}^{j} A_k^j P^k \right) \qquad \text{(A20)}$$

The approximation of the function F on E^n may also be written versus P^j according to :

$$\tilde{F} = \sum_{i=1}^{n} \sum_{j=1}^{i} c_i^* A_j^i P^j = \sum_{j=1}^{n} \sum_{i=j}^{n} c_i^* A_j^i P^j \qquad \text{(A21)}$$

in which n is the number of polynomials taken in the expansion of Rel. (A18).

Introducing the following notation :

$$K_p = \sum_{i=p}^{n} c_i^* A_p^i \qquad \text{(A22)}$$

Rel. (A21) may be rewritten as :

$$\tilde{F} = \sum_{p=1}^{n} K_p P^p \qquad \text{(A23)}$$

All the information concerning the chaotic attractor is therefore encoded in the set of coefficients K_p which forms a signature of the attractor. Hence, the set $\{K_p\}$ is called the natural spectrum of the attractor.